

Phase transitions in rare earth tellurides under pressure

This content has been downloaded from IOPscience. Please scroll down to see the full text.

2014 J. Phys.: Condens. Matter 26 274213

(<http://iopscience.iop.org/0953-8984/26/27/274213>)

View [the table of contents for this issue](#), or go to the [journal homepage](#) for more

Download details:

IP Address: 218.248.6.153

This content was downloaded on 31/08/2014 at 14:25

Please note that [terms and conditions apply](#).

Phase transitions in rare earth tellurides under pressure

L Petit¹, A Svane², M Lüders¹, Z Szotek¹, G Vaitheeswaran³, V Kanchana⁴ and W M Temmerman¹

¹ Daresbury Laboratory, Warrington WA4 4AD, UK

² Department of Physics and Astronomy, University of Aarhus, DK-8000 Aarhus C, Denmark

³ Advanced Centre of Research in High Energy Materials, University of Hyderabad, Professor C Rao Road, Gachibowli, Hyderabad 500 046, Andhra Pradesh, India

⁴ Department of Physics, Indian Institute of Technology Hyderabad, Ordinance Factory Estate, Yeddumailaram 502 205, Andhra Pradesh, India

E-mail: leon.petit@scfc.ac.uk

Received 2 January 2014, revised 12 February 2014

Accepted for publication 14 February 2014

Published 17 June 2014

Abstract

Using first-principles calculations we have studied the valence and structural transitions of the rare earth monotellurides $R\text{Te}$ ($R = \text{Ce, Pr, Nd, Pm, Sm, Eu, Gd, Tb, Dy, Ho, Er, Tm}$ and Yb) under pressure. The self-interaction corrected local spin-density approximation is used to establish the ground state valence configuration as a function of volume for the $R\text{Te}$ in both the NaCl (B1) and CsCl (B2) structures. We find that in ambient conditions all the $R\text{Te}$ are stabilized in the B1 structure. A trivalent (R^{3+}) rare earth ground state is predicted for the majority of the $R\text{Te}$, with the exception of SmTe , EuTe , DyTe , TmTe and YbTe , where the fully localized divalent (R^{2+}) rare earth configuration is found to be energetically most favourable. Under pressure, the trivalent $R\text{Te}$ undergo structural transitions to the B2 structure without associated valence transition. The divalent $R\text{Te}$ on the other hand are characterized by a competition between the structural and electronic degrees of freedom, and it is the degree of f-electron delocalization that determines the sequence of phase transitions. In EuTe and YbTe , where respectively the half-filled and filled shells result in a very stable divalent configuration, we find that it is the structural B1 \rightarrow B2 transition that occurs first, followed by the $R^{2+} \rightarrow R^{3+}$ valence transition at even higher pressures. In SmTe , DyTe and TmTe , the electronic transition occurs prior to the structural transition. With the exception of YbTe , the calculated transition pressures are found to be in good agreement with experiment.

Keywords: correlated electrons, rare earth materials, first-principles methodology

(Some figures may appear in colour only in the online journal)

1. Introduction

In the elemental rare earth metals, the sudden increase in lattice parameter at Eu and again at Yb [1] indicates that a distinction needs to be made between divalent rare earth ions $R^{2+}(f^n)$, with a fully localized f shell, and trivalent $R^{3+}(f^{n-1})$ ions, where one of the atomic f electrons delocalizes and takes

part in bonding. This dual character of the 4f electrons leads to the lanthanide compounds being characterized by very complex behaviour, and, for example, in the rare earth monochalcogenides the interplay of ligand chemistry and f-electron localization/delocalization results in an electronic phase diagram composed of metallic, semiconducting, and heavy fermion regions [2].

Of particular interest with respect to this phase diagram are the changes that occur under pressure. The rare earth chalcogenides all crystallize in the NaCl (B1) structure at ambient conditions, and with increasing pressure many of them

 Content from this work may be used under the terms of the [Creative Commons Attribution 3.0 licence](https://creativecommons.org/licenses/by/3.0/). Any further distribution of this work must maintain attribution to the author(s) and the title of the work, journal citation and DOI.

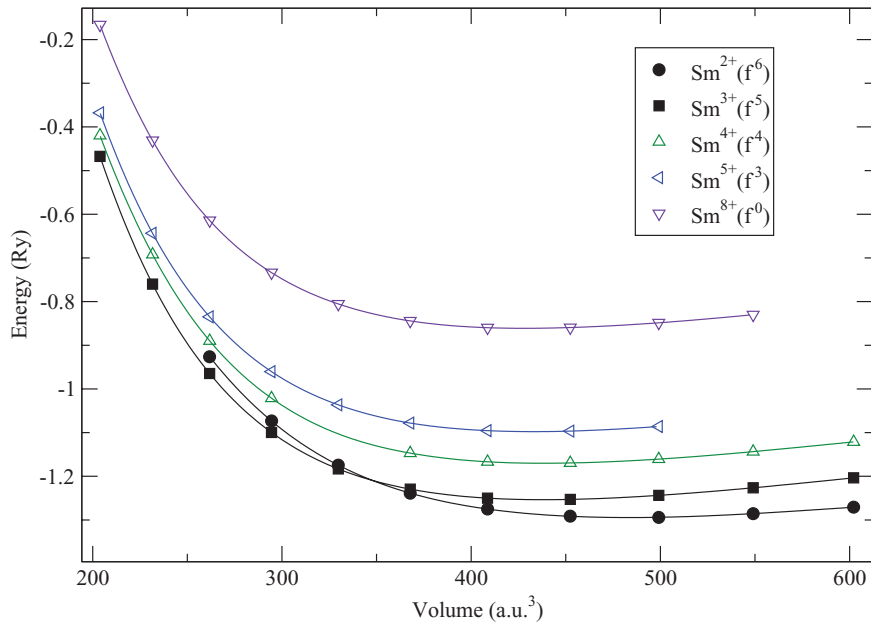


Figure 1. Total energies as a function of volume for the Sm^{2+} , Sm^{3+} , Sm^{4+} , Sm^{5+} and LSD configurations of SmTe in the B1 structure.

undergo a structural transition to the CsCl (B2) phase. For the majority of these compounds the rare earth configuration is trivalent at zero pressure, and it remains trivalent throughout the transition. However some of the Sm, Eu, Tm and Yb chalcogenides are characterized by divalent rare earth ground state configurations, and in these compounds a change in valence from $R^{2+}(f^n)$ to $R^{3+}(f^{n-1})$ can be brought about under pressure. It is well known for example that SmS , which at low temperature and zero pressure crystallizes in the NaCl structure with semiconducting behaviour, under moderate pressure of 0.65 GPa turns metallic with an associated significant volume collapse of 13.5% [3].

Depending on their equilibrium electronic structure, the rare earth chalcogenides thus undergo a combination of structural and valence transitions under pressure. In the present article we investigate this interplay between structural and electronic degrees of freedom, through a systematic study of the rare earth tellurides $R\text{Te}$ ($R = \text{Ce}, \text{Pr}, \text{Nd}, \text{Pm}, \text{Sm}, \text{Eu}, \text{Gd}, \text{Tb}, \text{Dy}, \text{Ho}, \text{Er}, \text{Tm}, \text{Yb}, \text{Lu}$). We use first-principles calculation to determine the ground state structure and valence from total energy considerations, and by following the evolution of the ground state as a function of pressure we predict the sequence of associated phase transitions.

2. Methodology

With respect to the theoretical studies, the local spin density (LSD) approximation to exchange and correlation fails to correctly describe the electronic structure of strongly correlated electron systems, and the rare earth tellurides with their localized 4f states are no exception to this rule. Applying the LSD based band picture to the 4f electrons results in narrow f bands situated at the Fermi level, predicting all the $R\text{Te}$ to be metallic. Consequently, the more recent calculations all use approximations that go beyond LSD when trying to

address the correlated nature of the f electrons. Here we use the so-called self-interaction corrected (SIC) local spin density (LSD) to predict the ground state properties of the $R\text{Te}$ from first principles. Hund's first and third rules are included in the self-consistency cycle, with the exchange interaction and the spin-orbit coupling explicitly added to the semi-relativistic one-particle Hamiltonian. With respect to the f electrons, Hund's second rule is taken into account by adding a so-called tetrad correction to the total energies. The electron wave functions are expanded in terms of the linear muffin-tin orbital (LMTO) basis functions [4], within the atomic sphere approximation (ASA). A full-potential correction is applied to corresponding B1 – B2 energy differences. In the following three subsections, these different corrections of the original LSD total energy will be described in detail.

2.1. SIC-LSD

In the LSD approximation the total energy functional is decomposed as

$$E^{\text{LSD}} = \sum_{\alpha}^{\text{occ.}} \langle \psi_{\alpha} | \hat{T} | \psi_{\alpha} \rangle + U[n] + V_{\text{ext}}[n] + E_{\text{xc}}^{\text{LSD}}[n_{\uparrow}, n_{\downarrow}], \quad (1)$$

where the sum runs over the kinetic energy, the Hartree energy, the interaction with the atomic ions, and the exchange and correlation energy. Like LSD, the SIC-LSD approximation is an effective one-electron density functional theory, albeit an orbital dependent one, obtained from the LSD total energy functional by removing the unphysical self-interaction of all the occupied/localized orbitals [5]. The SIC-LSD approach gives rise to split electron manifolds (here the 4f manifold), describing the dual character of electrons, represented by localized/occupied and hybridized/unoccupied subsets. The itinerant and localized limits are described by the same energy functional, which enables us to predict the ground state of

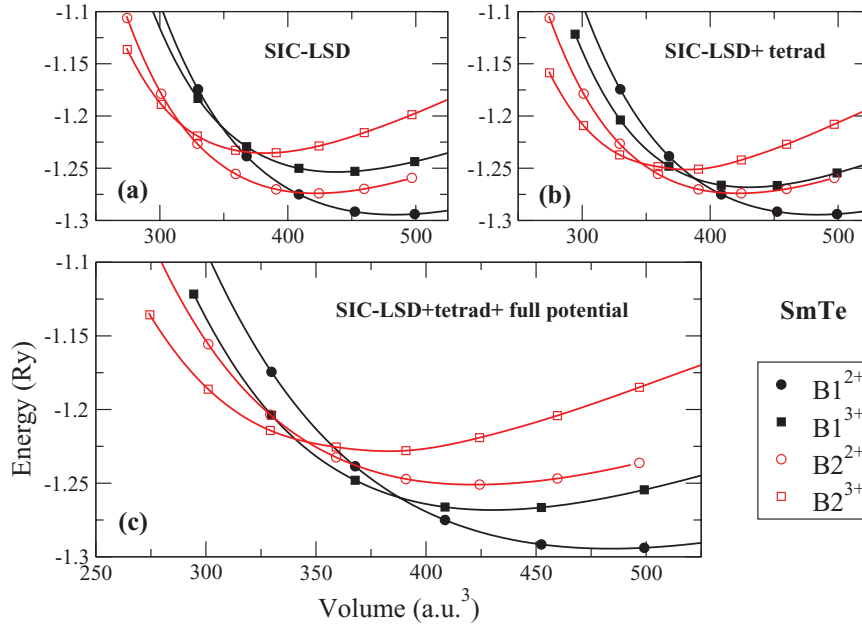


Figure 2. Total energies as a function of volume for SmTe. Energies are in Ry per formula unit and volumes in a.u.^3 . The black and red colours refer to the B1 and B2 structures respectively. $B1^{2+}$ and $B2^{2+}$ refer to the divalent $\text{Sm}^{2+}(f^6)$ configuration. $B1^{3+}$ and $B2^{3+}$ refer to the trivalent $\text{Sm}^{3+}(f^5)$ configuration. (a) SIC-LSD total energy calculation. (b) SIC-LSD total energies including the tetrad correction. (c) SIC-LSD total energies including the tetrad correction and the shift in energy of B2 relative to B1 due to the full-potential correction.

correlated electron materials from total energy considerations [6, 7]. The resulting, orbital dependent, SIC-LSD total energy functional has the form

$$E^{\text{SIC-LSD}} = E^{\text{LSD}} + E_{\text{so}} - \Delta E_{\text{sic}}, \quad (2)$$

where

$$\Delta E_{\text{sic}} = \sum_{\alpha}^{\text{occ.}} \delta_{\alpha}^{\text{SIC}} = \sum_{\alpha}^{\text{occ.}} \{ U[n_{\alpha}] + E_{\text{xc}}^{\text{LSD}}[\bar{n}_{\alpha}] \}, \quad (3)$$

$$E_{\text{so}} = \sum_{\alpha}^{\text{occ.}} \langle \psi_{\alpha} | \xi(\vec{r}) \vec{l} \cdot \vec{s} | \psi_{\alpha} \rangle. \quad (4)$$

The self-interaction energy (3) consists of the self-Coulomb and self-exchange-correlation energies of the occupied orbitals ψ_{α} with charge density n_{α} and spin density $\bar{n}_{\alpha} = (n_{\alpha}^{\uparrow}, n_{\alpha}^{\downarrow})$. For itinerant states, the self-interaction $\delta_{\alpha}^{\text{SIC}}$ vanishes identically, while for localized (atomic-like) states $\delta_{\alpha}^{\text{SIC}}$ may be appreciable. Thus, the self-interaction correction constitutes a negative energy contribution gained by an electron upon localization, which competes with the band formation energy gained by the electron if allowed to delocalize and hybridize with the available conduction states.

Hence, one can investigate localization phenomena in solids [8, 9] by realizing and studying different localization/delocalization scenarios, giving rise to different valence configurations, and through total energy minimization determine the ground state electronic structure and valence configurations of the compound under consideration. This nominal valence is defined as an integer number of electrons available for band formation

$$N_{\text{val}} = Z - N_{\text{core}} - N_{\text{SIC}}, \quad (5)$$

obtained by subtracting from the atomic number (Z) the sum of core (and semicore) (N_{core}) and SIC-localized (N_{SIC}) electrons.

Two uncoupled energy panels have been considered when constructing the LMTOs. The valence panel includes the 6s, 5d and 4f orbitals on the rare earth ion, and the 5s and 5p orbitals on Te, with all other orbitals downfolded [10]. The semicore panel comprises the 5s and 5p orbitals on the rare earth ion, as well as the 4d states on Te, with the remaining orbitals downfolded. Given the total-energy functional $E^{\text{SIC-LSD}}$, the computational procedure is as for the LSD case, i.e. minimization is accomplished by iteration until self-consistency. Determining the lowest-energy solution of the orbital functional (equation (2)) requires careful and thorough minimization with respect to both the number and symmetries of the localized orbitals [6, 11, 12]. The LS -coupling scheme is adopted for the localized f states by starting the iterations with Wannier states of appropriate symmetry. During iteration to self-consistency the symmetry of the Wannier states may change, although grossly retaining their overall characteristics due to the fact that the energy scale of spin-orbit interaction is smaller than that of exchange but larger than that of crystal fields for the f states.

For SmTe, the minimization procedure is demonstrated in figure 1. Here the total energy as a function of volume is shown for the B1 structure, assuming five different valence scenarios, namely $\text{Sm}^{2+}(f^6)$, $\text{Sm}^{3+}(f^5)$, $\text{Sm}^{4+}(f^4)$, $\text{Sm}^{5+}(f^3)$, and the fully delocalized LSD scenario $\text{Sm}^{8+}(f^0)$. The global energy minimum is obtained in the fully localized divalent $\text{Sm}^{2+}(f^6)$ configuration, with the corresponding equilibrium volume, $V_{\text{eq}} = 485 \text{ a.u.}^3$ in good agreement with the experimental value [13]. With respect to localized/delocalized scenarios, the trivalent $\text{Sm}^{3+}(f^5)$ configuration is closest in

energy, and at lower volumes, i.e. with increasing pressure, it does become the ground state. The increasingly delocalized scenarios from $\text{Sm}^{4+}(\text{f}^4)$ onwards are energetically unfavourable over the volume range considered here, and they play no role in the search for the ground state configuration of SmTe.

In figure 2(a), the Sm^{2+} and Sm^{3+} total energy configurations are depicted for both the B1 (black solid lines) and B2 (red solid lines) structures. For the NaCl structure the two configurations are represented by respectively B1^{2+} and B1^{3+} , whilst for the CsCl structure the corresponding configurations are denoted as B2^{2+} and B2^{3+} . Specifically for SmTe the divalent and trivalent configuration refer to the $\text{Sm}^{2+}(\text{f}^6)$ and $\text{Sm}^{3+}(\text{f}^5)$ valence configurations. Comparing the total energies, it can be seen from figure 2(a) that, in both the B1 and B2 structures, the energy minimum is obtained in the divalent $\text{Sm}^{2+}(\text{f}^6)$ scenario, with the global energy minimum in the B1^{2+} configuration, indicating that at ambient pressure SmTe is an insulator, crystallizing in the NaCl structure (stable relative to the CsCl structure).

From figure 2(a) it can furthermore be seen that with increasing pressure, i.e. with decreasing volume, the energy difference between the divalent B1^{2+} and the trivalent B1^{3+} configurations decreases, indicating that delocalizing an additional f electron becomes gradually more favourable. However we observe that B1^{3+} never actually becomes the ground state, and instead, around a volume of 400 a.u.³, the divalent CsCl structured (B2^{2+}) phase becomes energetically favourable. From this total energy behaviour, we would predict, based on the common tangent construction, that under pressure of 5.8 GPa a structural $\text{B1}^{2+} \rightarrow \text{B2}^{2+}$ transition occurs, from the divalent NaCl to the divalent CsCl structure. Upon further increasing the pressure, the trivalent B2^{3+} configuration becomes eventually more favourable energetically, indicating f-electron delocalization in the B2 phase at around 20 GPa. As we shall show however in the next two subsections, our analysis of the total energy versus volume behaviour will change dramatically once we take Hund's second rule and a full-potential correction into account.

2.2. Tetrad effect

In the Hartree–Fock approximation, the expectation value of the electron repulsion operator in some f^n multiplet state $\Psi^n(\text{LSJ})$ may be written as [14, 15]

$$\left\langle \Psi^n(\text{LSJ}) \left| \sum \frac{1}{r_{ij}} \right| \Psi^n(\text{LSJ}) \right\rangle = \frac{1}{2}n(n-1)E^0 + \alpha_1 E^1 + \alpha_2 E^2 + \alpha_3 E^3, \quad (6)$$

where $\Psi^n(\text{LSJ})$ in general is given by a linear combination of $n \times n$ Slater determinants. Since $\sum \frac{1}{r_{ij}}$ commutes with total L , S and J , the above matrix elements are equal for M_J quantum numbers belonging to one (LSJ) family. E^i are the Racah parameters [16], which are related to the Slater two-electron integrals (defined in equation (9)). The coefficients α_i depend on the choice of LSJ -configuration. The quantity E^0 is the

Coulomb repulsion between two f electrons, and the Coulomb energy term in the LSD total energy functional (1) corresponds to the $\frac{1}{2}E^0 n^2$ part of the first term in equation (6). The term $-\frac{1}{2}E^0 n$ in equation (6) cancels an equivalent contribution in the Hartree energy term, representing the interaction of an electron with itself; i.e. unlike the LSD approximation, the Hartree–Fock approximation is self-interaction free.

Of the remaining terms in equation (6), the E^1 term accounts for Hund's first rule. The E^2 term only contributes to the level spacing of excited multiplets and will not be relevant in a functional for the ground state energy. The E^3 term describes the level spacing between multiplets in the maximum spin configuration; i.e. this term accounts for Hund's second rule, by which the multiplet of maximum total orbital momentum, L , has the lowest energy. With respect to the average f^n (maximum spin) energy (the grand barycentre), the maximum L multiplet is lowered by $-jE^3$, where $j = (0, 9, 21, 21, 9, 0, 0)$ for $n = (1-7)$ and $n = (8-14)$ respectively. It is an atomic effect which results in an increased stability at one-quarter and three-quarters filling of the 4f shell, and this second Hund's rule effect is often referred to as the tetrad effect (TE) [15]. Although both LSD and SIC-LSD take into account Hund's first and third rules, with respectively the exchange interaction and spin–orbit coupling included in the total energy functional, Hund's second rule is not accounted for in the homogeneous electron gas, which is the underlying reference system of the LSD [17]. To account for it in our total energy calculations, we add (*a posteriori*) to the SIC-LSD total energy functional the relevant correction

$$\Delta E_t = -jE^3. \quad (7)$$

The E^3 parameter is equivalent to Racah's B -parameter, [16] and is given in terms of the reduced Slater integrals F_k as

$$E^3 = \frac{1}{3}(5F_2 + 6F_4 - 91F_6), \quad (8)$$

where $F_k = F^k/D^k$. Here D^k are numerical constants ($D^k = 225, 1089, 7361.64$ for $k = 2, 4, 6$) and the Slater integral F^k is defined through

$$F^k = e^2 \int_0^\infty \int_0^\infty \frac{(r_<)^k}{(r_>)^{k+1}} \phi_{4f}^2(r_1) \phi_{4f}^2(r_2) r_1^2 dr_1 r_2^2 dr_2. \quad (9)$$

Here, ϕ_{4f} is the f-partial wave as calculated in the self-consistent crystal potential, and $r_< (r_>)$ denotes the smaller (larger) of the variables r_1 and r_2 . In reality, correlation effects in the solid environment tend to reduce the multiplet energy level splittings. Hence our calculated TE values are on average 15–20% larger than their experimental counterparts [15].

In figure 2(b) the total energy as a function of volume is again depicted for SmTe but with the total energies now corrected by the tetrad contribution ΔE_t . The most noticeable change compared to figure 2(a) is that, for both the B1 and B2 structures, the energy difference between the divalent and trivalent configurations is considerably reduced. The correction is largest at small volumes, where it reaches 40 mRy. For large volumes it reduces to 10 mRy. Note that for SmTe the global energy minimum even after the tetrad correction remains solidly B1^{2+} .

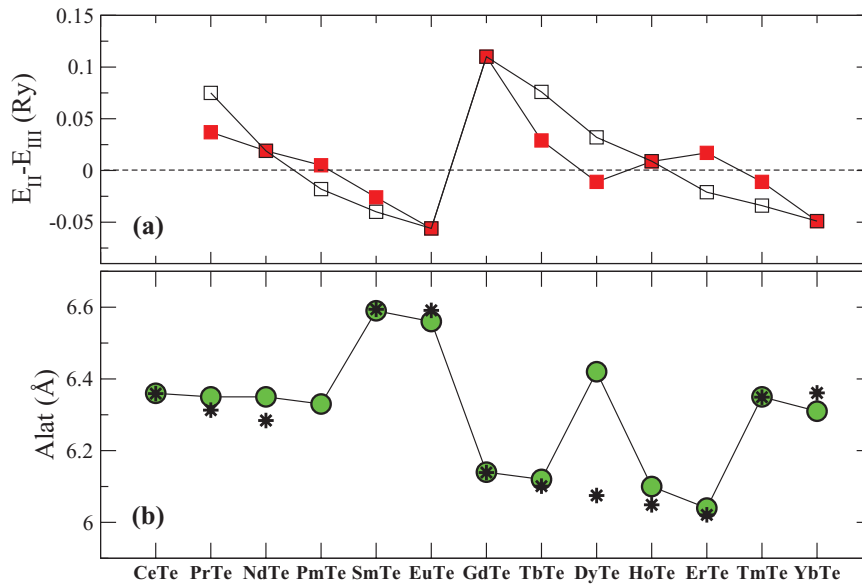


Figure 3. Ground state properties of the rare earth tellurides. (a) Energy difference between divalent and trivalent configurations, $E_{II}-E_{III}$. The open (filled) squares give the energy difference without (with) tetrad correction. (b) Comparison of theoretical (filled spheres) and experimental (asterisks) lattice parameters.

2.3. Full potential correction

As mentioned earlier, in the present work, the electron wave functions are expanded in terms of the LMTO basis functions [4], within the ASA, whereby the crystal volume is divided into slightly overlapping atom centred spheres of a total volume equal to the actual volume. To improve the packing of the NaCl structure, empty spheres have been introduced on high-symmetry interstitial sites. A well known shortcoming of ASA is that different crystal structures have different degrees of overlap of the ASA spheres, resulting in substantial relative errors in the evaluation of the total energy. In a full-potential implementation the problems associated with ASA do not occur, as all the non-spherical contributions to the potential are included, and no shape approximation to the crystal geometry is invoked.

Unfortunately, the SIC-LSD is as yet not implemented in a full-potential version. However, the relative error introduced by the ASA can be estimated from a comparison of the total energies as obtained respectively with a full-potential method and the ASA calculation, when both are applied to the f^0 (LSD) configuration. Thus, within the LSD approximation, the total energy difference between the NaCl and CsCl structures derived by means of the full-potential calculations can be used to calibrate the corresponding energy difference derived from the ASA calculations. Whilst the ASA inhibits the comparison of energies of different crystal structures, the ASA error is of minor influence when comparing the energies of different localization scenarios (here $Sm^{2+}(f^6)$ and $Sm^{3+}(f^5)$) within the same crystal structure. The energy calibration derived for the LSD scenario can therefore be applied globally to the NaCl versus CsCl energies, and results in a rigid shift of the B1 energy curves with respect to the B2 energy curves. From the full-potential LMTO [18] calculations, it emerges that this shift varies between 20 and 30 mRy

depending on the rare earth telluride. Given the approximative nature of this correction, in the following we apply a constant 20 mRy shift to B2 total energies, representing a lower limit to the full-potential correction.

The result of this correction is demonstrated for SmTe in figure 2(c), where compared to figure 2(b) the B2 curves have moved towards higher energy relative to the B1 curves. The resulting phase diagram in figure 2(c) (which also incorporates the lowering of the trivalent configurations relative to the divalent configurations due to the tetrad effect) differs significantly from the uncorrected phase diagram depicted in figure 2(a). Now, with decreasing volume, around 375 a.u.³, and whilst remaining in the NaCl phase, the trivalent Sm^{3+} becomes energetically most favourable. The CsCl structure is only stabilized at smaller volumes of around 325 a.u.³. From the common tangent construction, we find that under pressure an isostructural, $B1^{2+} \rightarrow B1^{3+}$, localization–delocalization transition occurs at around 9.5 GPa, followed at higher pressures, around 12 GPa, by a structural, $B1^{3+} \rightarrow B2^{3+}$, transition.

3. Results

3.1. Ground state properties

The ground state properties of the rare earth chalcogenides in the NaCl structure have previously been studied extensively by means of SIC-LSD calculations [2, 8, 19–24]. The calculated differences, $E_{II}-E_{III}$, between the energy minima of the divalent $B1^{2+}$ and trivalent $B1^{3+}$ configurations for the entire rare earth telluride series are summarized in figure 3(a). Here a positive energy difference indicates that the ground state is trivalent, whilst a negative energy difference implies a fully localized divalent ground state. The divalent configuration is predicted to be the ground state for SmTe, EuTe, TmTe and

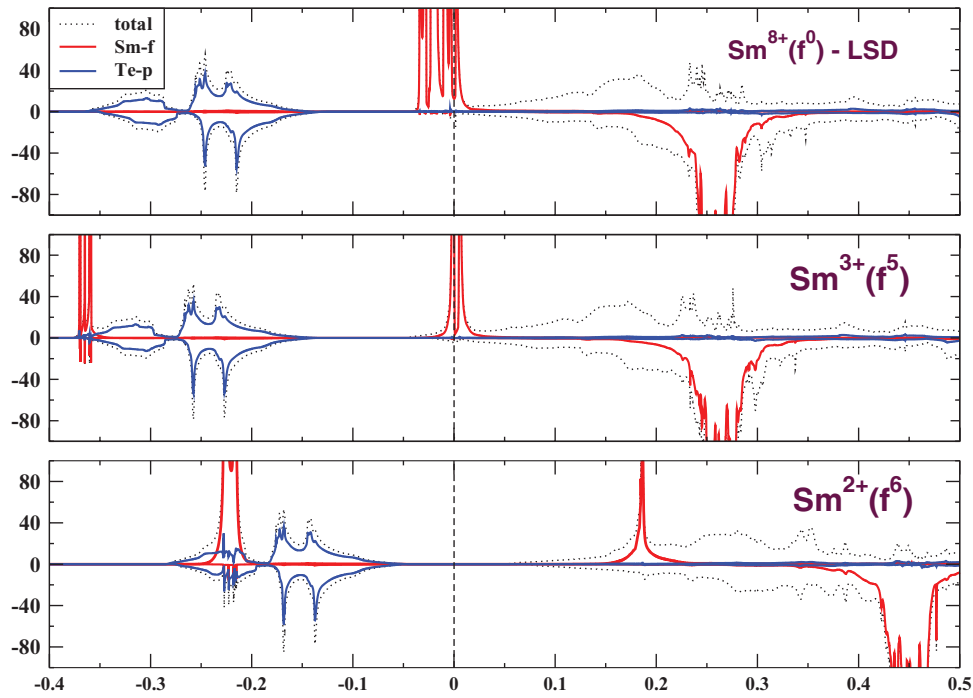


Figure 4. DOS of SmTe. (a) LSD; (b) trivalent configuration; (c) divalent configuration. The Fermi level is indicated by the vertical dashed line. Energies are in Ry, DOSs are in states per Rydberg and per formula unit. Note that the majority (minority) spin component is shown along the positive (negative) direction of the second axis.

YbTe, as well as DyTe. In figure 3(a) the open squares refer to the total energy differences prior to the tetrad correction. The effect of the latter is most notable for PmTe, DyTe and ErTe, where it changes the predicted ground state. In figure 3(b) the calculated equilibrium lattice parameters of the corresponding ground state configurations are compared to their experimental counterparts. The agreement is rather good, including the overall trend towards smaller lattice parameters with increasing rare earth ion size, which is a reflection of the lanthanide contraction. The sudden jump in lattice parameter at EuTe and SmTe, as well as TmTe and YbTe, is a result of the corresponding divalent ground state configuration in figure 3(a), with the $R^{3+} \rightarrow R^{2+}$ localization transition leading to decreased bonding and increased lattice parameters. From figure 3(a), we notice that DyTe becomes divalent as a result of the tetrad correction. The resulting lattice parameter increase that we predict is not observed experimentally, as can be seen quite clearly in figure 3(b). A possible explanation for this discrepancy could be that in some cases we overestimate the TE's influence as a result of approximating the respective Slater integrals by the fully localized atomic limit instead of also considering the corrections due to the solid-state environment (screening/hybridization). On the other hand, this overestimation cannot be severe, given that an earlier SIC-LSD study of all 130 rare earth monpnictides and monochalcogenides [2] has shown that DyTe is the only compound where the predicted lattice parameter is found to disagree with experiment. Furthermore, the calculated total energy difference for DyTe is only 11 mRy per formula unit, in favour of the divalent configuration.

In figure 4, the density of states (DOS) for SmTe is shown. Figure 4(a) corresponds to the LSD result, with all

the electrons, including the 4f states, treated as delocalized band states. The latter are pinned to the Fermi level, predicting SmTe to be a metal, in disagreement with experiment. The electron–electron interactions, that tend to localize the strongly correlated f electrons, are not fully taken into account within LSD, which in the SIC-LSD calculations manifests itself by the scenario in figure 4(a) being energetically very unfavourable. In the $\text{Sm}^{3+}(\text{f}^5)$ scenario of figure 4(b), the SIC has been applied to five of the Sm 4f electrons, that are now treated as localized, situated just below the Te p states in the corresponding DOS. One of the f electrons remains delocalized, and situated at the Fermi level, i.e. SmTe remains metallic in the Sm^{3+} scenario. Localizing all six Sm f electrons results in the divalent $\text{Sm}^{2+}(\text{f}^6)$ scenario of figure 4(c). Energetically, we find this to be the ground state for SmTe, i.e. more favourable than the $\text{Sm}^{3+}(\text{f}^5)$ configuration by 26 mRy.

From figure 4(c) we find SmTe to be an insulator with an energy gap of 1.3 eV (0.096 Ry). The localized f states are found to be situated at 3.6 eV below the conduction band minimum. It is important to notice that the focus of the SIC-LSD approach is on total energies. It is after all a one-electron ground state theory, which does not give accurate removal energies of localized states due to electron–electron interaction (multiplet) effects [25] and the neglect of screening and relaxation effects [26], and in the case of SmTe these occupied f states appear as sharp resonances unrealistically far below the conduction band minimum (–10 eV for SmTe). A rough estimate of the removal energies may be obtained by the transition state argument [27], which places the f peak midway between its calculated SIC-LSD and LSD positions, and which is the approach that was adopted in figures 4(b) and (c). This places the f peak at 3.5 eV below the conduction band

minimum, which is still a long way off the experimentally determined position, i.e. situated in the Te(p)–Sm(d) energy gap at 0.7 eV below the conduction band minimum [28]. An improved approach to taking into account the missing screening/relaxation effects might be through a so-called Δ_{SCF} calculation [29, 30], or potentially most rewarding by combining the SIC with the GW approach [31].

A popular method for making contact with spectroscopy is the LDA+ U approach [32]. Guided by experiment, i.e. once the ground state is known to be insulating, an effective Coulomb parameter U is introduced that separates the LSD f manifold into lower and upper Hubbard bands and removes the f degrees of freedom from the Fermi level. Given that U is an adjustable parameter, good agreement with photoemission measurements can be achieved [33, 34]. The combination of dynamical mean field theory (DMFT) with LDA+ U has resulted in what currently represents the most successful electronic structure methodology for reproducing the electronic excitations of strongly correlated materials [35], although as far as the majority of applications to date is concerned the methodology inherits the uncertainties of LDA+ U , most notably the effective U and the double counting correction [36]. Using an empirical model instead of first-principles calculations, Rogers *et al* [37] successfully predicted the ground state electronic properties of the rare earth tellurides.

Compared to LDA+ U /DMFT, the strength of the SIC-LSD lies with predicting the ground state electronic structure from first principles, i.e. without having to rely on adjustable parameters or prior experimental evidence. As we shall see in the following section, this predictive capability becomes especially useful when considering changes in electronic structure under pressure. Although assuming U to remain constant under pressure can be an acceptable approximation in some cases, in general there is no well defined and/or justified approach to describing changes of U under pressure, and therefore an insulator (large U) to metal ($U \sim 0$) transition cannot be adequately represented. The SIC-LSD method, at any given pressure, determines the ground state by distinguishing between localized (insulator) and delocalized (metal) f -electron states, based on the corresponding total energies.

3.2. Transition pressures

The calculated transition pressures and associated volume collapses for the rare earth tellurides are presented in table 1. The divalent compounds SmTe, EuTe, TmTe and YbTe are by far the most interesting with respect to changes under pressure, as is also reflected by the large number of experimental studies of these compounds.

Experimental investigations on SmTe find an anomalous pressure–volume behaviour whilst retaining the NaCl structure, which is associated with a continuous isostructural valence change. The various measurements differ somewhat on the onset and range of the transition [38–42], with for example early measurements by Chatterjee *et al* [38] indicating a pressure range of 2–6 GPa, whilst in later measurements Le Bihan *et al* [41] determined the range to be 6–8 GPa. The

SIC-LSD total energy calculations predict a $B1^{2+} \rightarrow B1^{3+}$ valence transition to occur around 9.5 GPa, with a volume collapse of 7.6% accompanying the associated insulator to metal transition. The calculated transition pressure is thus at the upper end of the experimental pressure range. The sluggishness of the observed transitions is not found in the theory, and might reflect a finite temperature effect. Using an *ab initio* pseudopotential method (SIESTA) with GGA to account for exchange and correlation, and two different sets of pseudopotentials to describe the divalent and trivalent Sm configurations, Gupta *et al* [43] predict a valence transition to occur at 7.1 GPa. The insulator to metal transition is not found in this approach, as the localized character of the f electrons is not taken into account within GGA.

At a pressure of around 12 GPa SmTe is seen to undergo a structural transition from the NaCl to the CsCl structure. Thus Chatterjee *et al* [38] determine a transition pressure of 11 GPa with a volume collapse of 9.1%, whilst Le Bihan *et al* [41] determine the transition pressure to be 12.9 GPa with an associated volume collapse of 6.8%. From the SIC-LSD calculations we derive a transition pressure of 12.3 GPa, in good agreement with these experimental values. The calculated volume collapse of 11.3% is slightly larger than is observed experimentally.

Based on x-ray diffraction and resistivity measurements, Rooymans [44] determined that under pressure EuTe undergoes an isostructural phase transition at around 1.5 GPa, with an associated volume collapse of 5%. According to the author, the high pressure phase remains B1, with the Eu transforming from the divalent to the trivalent configuration. On the other hand, Singh *et al* [45] in their high pressure x-ray diffraction study determined that no noticeable change in valence occurred up to pressures of 10 GPa, where a structural transition to the CsCl structure is observed. In a neutron diffraction study on EuTe, Goncharenko *et al* [46] determined the onset of the B1 to B2 transition around 13 GPa, with the two phases coexisting up to 17 GPa. In the whole pressure range investigated, the ratio of magnetic and nuclear intensities is found to agree with ordered Eu^{2+} magnetic moments. Reflectivity measurements up to a pressure of 30 GPa in the B2 phase of EuTe did not show any noticeable changes in optical properties that could be associated with a change in valence state [13]. In good agreement with these latter experimental data, our calculations predict a structural $B1^{2+} \rightarrow B2^{2+}$ transition around 13 GPa, with an isostructural $B2^{2+} \rightarrow B2^{3+}$ valence transition only setting in at significantly higher pressures of around 47 GPa. A number of theoretical studies have focused on the NaCl to CsCl structural transition in EuTe [47], with calculated transition pressures ranging from 10 to 17 GPa. In these studies exchange and correlation is mostly taken into account at the LDA or GGA level; the rather good agreement with experiment indicates that the electronic structure associated with the fully occupied majority-spin f band of the Eu^{2+} configuration can be reasonably described without taking into account the localized character of the f electrons. This is of course no longer the case when f -electron delocalization from Eu^{2+} to Eu^{3+} sets in under pressure.

Table 1. Structural and electronic transition pressures.

<i>R</i> Te	SIC-LDA			Experiment	
	Transition	Pressure (GPa)	$\Delta V/V$ (%)	Pressure (GPa)	$\Delta V/V$ (%)
CeTe	B1 ³⁺ → B2 ³⁺	4.8	12.5	8.0±1.0 ^b	8.5
	B2 ³⁺ → B2 ⁴⁺	41.7	5.0	—	—
PrTe	B1 ³⁺ → B2 ³⁺	9.5	11.1	9.0±1.0 ^a	11.5
NdTe	B1 ³⁺ → B2 ³⁺	22.9	11.9	—	—
PmTe	B1 ³⁺ → B2 ³⁺	8.1	12.1	—	—
SmTe	B1 ²⁺ → B1 ³⁺	9.6	7.6	3.0–6.0 ^d ;6.0–8.0 ^e ;4.6–7.5 ^f	cont. 11 ^d
	B1 ³⁺ → B2 ³⁺	12.3	11.3	11.0 ± 1.0 ^d ;12.9 ^e	9.1 ^d ;6.8 ^e
EuTe	B1 ²⁺ → B2 ²⁺	13.0	10.0	11 ^a , 13–17 ^g	11.6 ⁱ
	B2 ²⁺ → B2 ³⁺	47.3	4.0	—	—
GdTe	B1 ²⁺ → B1 ³⁺	—	—	1.5 ^h	5.0 ^h
	B1 ³⁺ → B2 ³⁺	25.2	—	—	—
TbTe	B1 ³⁺ → amorph.	—	—	15–35 ^c	—
	B1 ³⁺ → B2 ³⁺	9.5	11.0	—	—
DyTe	B1 ²⁺ → B1 ³⁺	3.1	11.3	—	—
	B1 ³⁺ → B2 ³⁺	13.4	10.0	—	—
HoTe	B1 ³⁺ → B2 ³⁺	46.6	—	—	—
	B1 ³⁺ → amorph.	—	—	40–50 ^c	—
ErTe	B1 ³⁺ → B2 ³⁺	12.7	10.8	—	—
TmTe	B1 ²⁺ → B1 ³⁺	2.9	12.1	2–6 ^{k,l}	cont. 10(1) ^d ;8 ^k
	B1 ³⁺ → B2 ³⁺	14.9	9.9	—	—
YbTe	B1 ³⁺ → tetrag.	—	—	8 ^{j,k}	—
	B1 ²⁺ → B2 ²⁺	17.7	9.2	—	—
	B2 ²⁺ → B2 ³⁺	31.1	4.4	—	—
	B1 ²⁺ → B1 ³⁺	—	—	15–20 ^m	8 ^m
	B1 ²⁺ → amorph.	—	—	48–60 ^c	—

^a [45]. ^b [48]. ^c [49]. ^d [38]. ^e [41]. ^f [39]. ^g [46]. ^h [44]. ⁱ [13]. ^j [50]. ^k [51]. ^l [52]. ^m [53].

TmTe at ambient conditions is found experimentally to be an insulator crystallizing in the NaCl structure. At pressures of around 2 GPa, an isostructural transition occurs associated with a valence change from the divalent Tm²⁺ configuration to an intermediate valent Tm²⁺/Tm³⁺ metallic state. The intermediate valence state is characterized by Kondo-like behaviour and f–d hybridization [52, 54], with possibly reentrant insulating behaviour around 7 GPa [54]. At 8 GPa a structural transition to a tetragonal metallic phase is observed [50, 51]. The latter is characterized as close to trivalent [54]. The SIC-LSD calculations predict an insulator to metal transition to occur at around 3 GPa, in very good agreement with experiment. With respect to the structural transition, similar to all earlier cases, we investigated the B1 → B2 transition, which we estimated to occur around 15 GPa. We did not attempt to model the actual transition from the B1 to the tetragonal structure that occurs around 8 GPa, and it is not obvious whether the B2 structure will occur at $P > 8$ GPa [50, 55]. The theory results for TmTe are summarized in figure 5.

YbTe under pressure was investigated by Chatterjee *et al* [53] by means of high pressure x-ray diffraction up to 30 GPa. They observed that the structure remains NaCl throughout the pressure region, and associate the anomalous pressure–volume behaviour in the region around 15–20 GPa with an Yb²⁺ → Yb³⁺ electronic collapse. Absorption [56] and photoconductivity [57] measurements suggest an energy for the 4f–5d delocalization transition around 2 eV, which based on the change in activation energy as a function of pressure suggests a transition pressure of 15 GPa. Resistivity measurements [58] suggest a smaller value for the f–d gap of around

0.5 eV, which would indicate gap closure under a pressure of around 4 GPa. Recent measurements on YbTe by means of high-pressure x-ray diffraction do not show the pressure induced valence change [49]. No discontinuity was observed in the 10–20 GPa range of the compression curve, and neither are there signs of a B1 to B2 transition up to 48 GPa, where decomposition and amorphization apparently sets in. As can be seen from table 1, our calculations are at odds with the experimental measurements, as we predict a structural B1²⁺ → B2²⁺ transition to occur around 17 GPa. The electronic transition from Yb²⁺ to Yb³⁺ is predicted to occur within the B2 structure at a pressure of 31 GPa. The calculated transitions are very similar to the ones predicted earlier for EuTe. In the ground state of both compounds, the divalent configuration is found to be energetically very favourable compared to the trivalent configuration. The resulting stability towards f-electron delocalization causes the structural transition to occur first under pressure.

High-pressure x-ray studies have shown that CeTe undergoes a structural transition from the B1 to B2 structure at pressures of around 8 GPa, with a volume change of 8.5%. The reversed transition on decreasing pressure occurs around 3 GPa [59]. The calculated transition pressure (4.8 GPa) is lower than the experimental value but within the hysteresis pressure range. The ground state configuration on both sides of the transition is trivalent. At higher pressure, around 41 GPa, the calculations predict a valence transition from Ce³⁺ to Ce⁴⁺ to occur in the CsCl phase of CeTe. No experiments have been performed beyond 25 GPa [59].

PrTe, which at ambient pressure is in the trivalent ground state configuration, is seen experimentally to undergo a

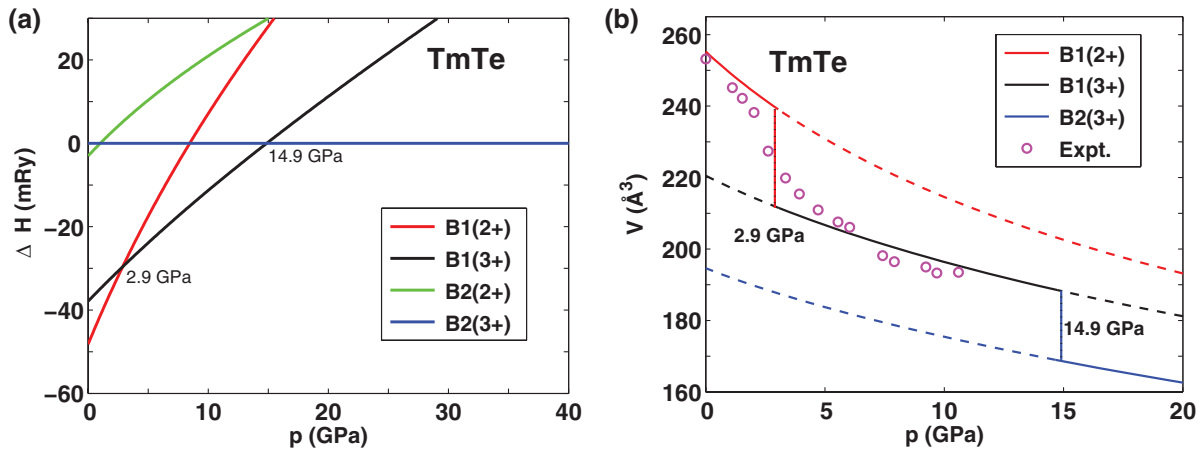


Figure 5. The theoretical behaviour of TmTe under pressure. (a) The enthalpies of the structures B1 and B2 with Tm configuration 3+ or 2+. The enthalpy of B2(3+) is used as reference. The calculated transition pressures for B1(2+) \rightarrow B1(3+) and for B1(3+) \rightarrow B2(3+) are quoted. (b) The calculated p - V relation of TmTe. The full lines give the predicted sequence of B1(2+), B1(3+) and B2(3+) phases, while the dashed lines are extensions of the p - V relations beyond the respective transition pressures. The experimental data of [54] are shown with pink circles.

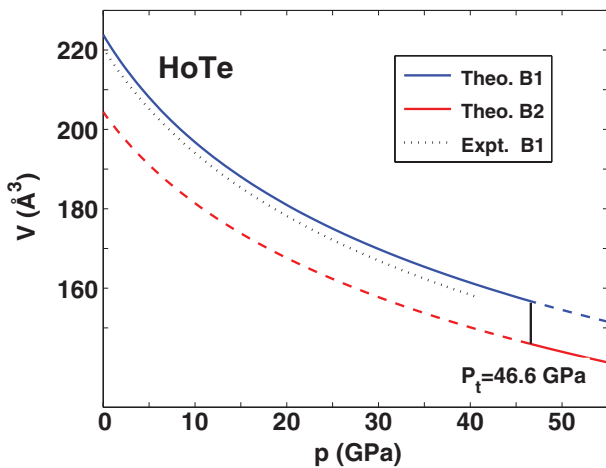


Figure 6. Volume versus pressure behaviour for HoTe. The blue and red curves indicate the calculated results for respectively the B1 and B2 structures. The dotted line depicts the experimentally observed data from [49].

structural transition to the CsCl phase around 9 GPa. Our calculations predict this same transition to occur at 9.5 GPa with an associated volume collapse of 11%.

HoTe and GdTe have only very recently been investigated by means of high-pressure x-ray diffraction [49]. No structural transition from the B1 to B2 structure was observed in either of the compounds up to the maximum pressures attained. Instead decomposition and amorphization occurs, for GdTe in the range of 18–35 GPa and for HoTe in the range of 40–50 GPa. The authors explain this so-called pressure induced amorphization as being due to the fact that the material fails to reach a higher density stable phase and ends up in a disordered structure. The SIC-LSD calculations predict a structural B1³⁺ \rightarrow B2³⁺ transition for both GdTe and HoTe, occurring respectively at 25.2 GPa and 46.6 GPa. The calculated and experimentally observed pressure versus volume behaviours for HoTe are compared in figure 6. It is of course

possible that the amorphous, disordered, phase turns out to be energetically more favourable than the ordered CsCl phase. This however cannot be investigated within the framework of band structure theory, but rather would require the use of a molecular dynamics based approach.

With respect to the remaining rare earth tellurides, NdTe, PmTe, DyTe and ErTe, we are not aware of experimental high-pressure investigations on these compounds. Our calculated transition pressures will thus have to wait for experimental confirmation. For DyTe, we predict a B1²⁺ \rightarrow B1³⁺ electronic transition to occur at 3 GPa. This is due to the fact that we wrongly predict a divalent ground state, and it is safe to assume that this transition will not be observed experimentally. Instead starting from the DyTe trivalent configuration, we expect only the corresponding structural B1³⁺ \rightarrow B2³⁺ transition in table 1 to occur (at 13.4 GPa).

It should be noted here that in earlier SIC-LSD calculations slightly different transition pressures were found for the valence transition in SmTe (6.2 GPa) [23, 24] and TmTe (8 GPa) [21], and the structural transition in CeTe (7.4 GPa) [22, 60] and PrTe (5 GPa) [61]. In those calculations, neither the tetrad effect nor the full-potential correction were taken into account.

3.3. Structural and electronic transitions

The structural transition from the sixfold coordinated B1 to the eightfold coordinated B2 structure is observed in a large number of compounds. Studies on the alkaline earth chalcogenides have shown that the transition pressure decreases with increasing cation or anion radius [62]. With the telluride anion radius constant throughout the series, and the cation radius decreasing ever so slowly from Ce to Yb [63], we would expect a slow increase in structural transition pressure from CeTe to YbTe. The trend in calculated transition pressures as a function of $R\text{Te}$ plotted in figure 7 does show a moderate increase, with the exception of NdTe and HoTe, that lie

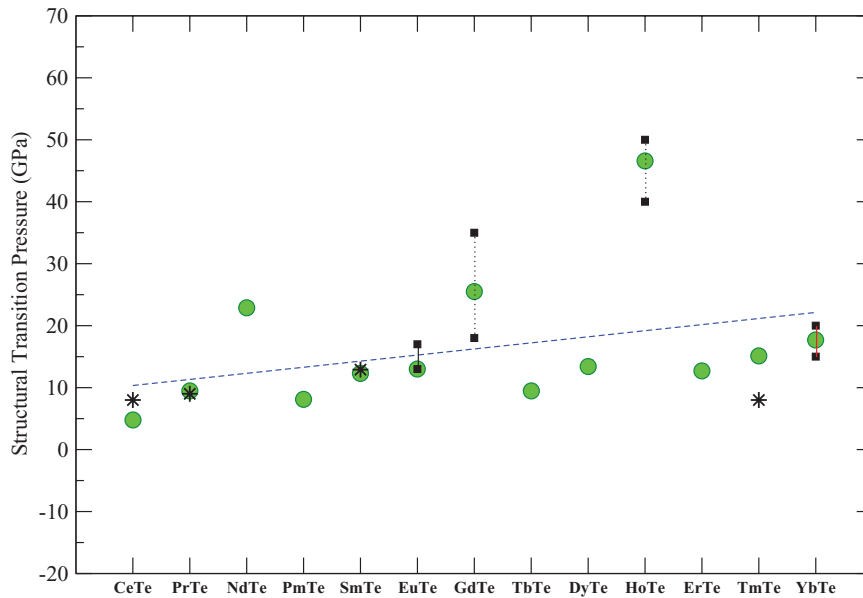


Figure 7. Structural B1 \rightarrow B2 transition pressures for the rare earth tellurides. The green circles refer to the theoretical data, the black stars to the experimental values. Dotted vertical lines indicate the pressure range for amorphization. The red vertical line refers to the pressure range for the experimentally observed valence transition in YbTe. The experimental pressure for TmTe refers to the B1 to tetragonal transition.

rather far off the linear regression line. Noticeably for EuTe and YbTe, where the calculations indicate a structural transition occurring in the divalent phase, there is no indication of a sudden lowering of the transition pressure, as one might otherwise expect from the fact that the R^{2+} radii are larger than the R^{3+} radii. A possible drop in transition pressure in connection with the structural transition in EuTe is also not observed experimentally. YbTe does not undergo a structural transition up to the highest pressures registered.

From photoemission experiments it has been established that in the divalent compounds SmTe, EuTe, TmTe and YbTe the localized f states are situated in the gap separating the occupied Te p from the unoccupied rare earth 5d states. The accepted view is that under pressure the f–d gap starts closing, and that at the transition point where the gap closes f \rightarrow d transfer or f–d mixing brings about a change in valence. Experiments have shown that this valence change is not sudden and complete from 2+ to 3+, but rather to an intermediate valence [38, 54, 59], gradually increasing with increasing pressure.

In SIC-LSD the valence transition in SmTe occurs at 9.6 GPa. In terms of the corresponding change in electronic structure, it can be visualized as a ground state transition from the divalent configuration depicted in figure 4(c) to the trivalent configuration depicted in figure 4(b). With the spectroscopy of the f states not being correctly reproduced, we cannot say whether just before the transition the f–d optical absorption gap closes, but we do find that the intrinsic p–d semiconductor gap reduces from 1.2 to 0.6 eV when increasing the pressure from zero to 9.6 GPa. From the DOS in figure 4(b) we see that the Fermi level cuts across the f peak, indicating that apart from the five localized f states a fractional number of delocalized f electrons is present in the nominally

trivalent phase. The f–d transfer is thus not complete, and the actual trivalent ground state can be described as intermediate, or fluctuating $\text{Sm}^{2+}/\text{Sm}^{3+}$, where we can associate the number n_f of occupied f-band states with the fraction of Sm^{2+} ions, $|\psi(\text{Sm})\rangle \sim (1 - n_f)|\text{Sm}(3+)\rangle + n_f|\text{Sm}(2+)\rangle$.

It emerges that the number of delocalized f states eventually determines the ground state. In SmTe for example, for n_f large, the narrow f peak in figure 4(b) is close to completely filled. This leads to a marginal gain in band formation energy and, given the relative strength of the competing electron–electron interactions, the corresponding state prefers to localize, gaining the associated SI energy. The resulting SmTe ground state is divalent. With increasing f–d charge transfer n_f becomes smaller, as a result of the f peak emptying in favour of the broader d band, and band formation becomes increasingly favourable. Eventually, the trivalent scenario depicted in figure 4(b) becomes the ground state, at 9.6 GPa. A very similar picture applies to EuTe, DyTe, TmTe and YbTe, that as we have shown earlier also prefer the fully localized divalent f-electron manifold at equilibrium, and undergo a delocalization transition under pressure. The number n_f where this transition occurs is to some degree dependent on the chemistry, but has been shown earlier to be situated around 0.65 ± 0.05 electrons [60, 64].

This dependence of the ground state configuration on the number of delocalized f states is visualized in figure 8, where we have plotted n_f as a function of pressure, for PrTe, SmTe and EuTe in the nominally trivalent configuration. The horizontal dotted line indicates the limit of 0.65 electrons. We see that for PrTe, in both the B1 and B2 structures, n_f is smaller than 0.6 already at zero pressure, which results in a trivalent ground state. For SmTe, n_f crosses the dotted line around 10 GPa, which as we have seen earlier is in the pressure range

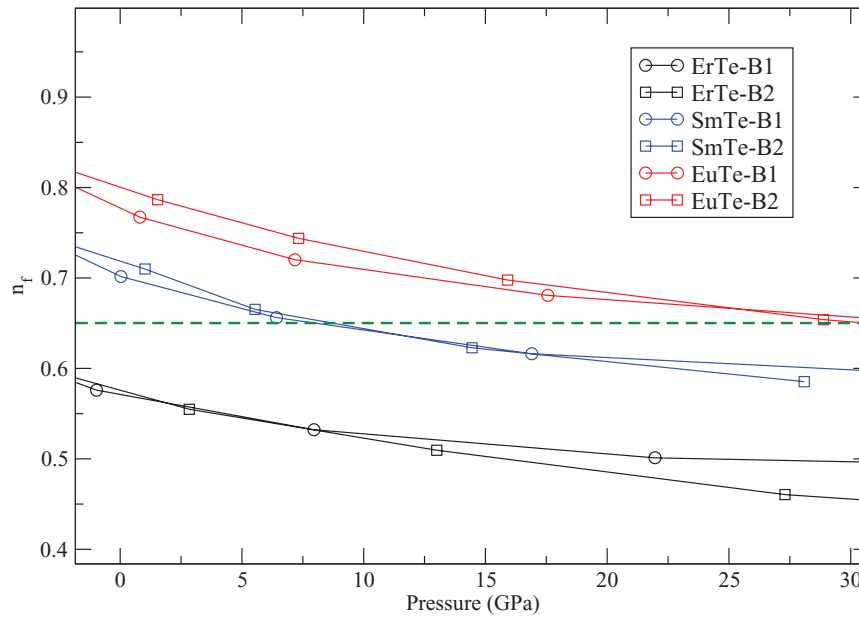


Figure 8. The number n_f of delocalized f electrons in both the B1 and B2 structures as a function of pressure. The red, blue and black colours refer to ErTe, SmTe and EuTe respectively.

where the $B1^{2+} \rightarrow B1^{3+}$ transition is observed. Finally, in EuTe, the number of delocalized f states stays above 0.65 for pressures beyond 30 GPa, in both the B1 and B2 structures. Here at 13 GPa a $B1^{2+} \rightarrow B2^{2+}$ transition is observed, whilst the divalent to trivalent transition occurs at much higher pressure. Thus indirectly, if n_f is close to unity at equilibrium, i.e. the f peak is almost completely filled, then the divalent configuration is stable to such a degree that it survives beyond the structural transition.

4. Conclusion

Using first-principles calculations, we have studied the structural and electronic transitions that occur under pressure in the rare earth monote tellurides. We find that at ambient pressure the NaCl structure is stable relative to the CsCl structure. The corresponding ground state electronic structures are determined by the degree of f-electron localization, which increases from CeTe to EuTe, and again from GdTe to YbTe, resulting in the fully localized divalent configuration becoming energetically favourable for SmTe, EuTe, DyTe, TmTe and YbTe, whilst the remaining tellurides prefer the trivalent ground state configuration. Under pressure the latter undergo a structural NaCl to CsCl transition, whilst the divalent compounds undergo a combination of structural and valence transitions, with the relative order of these transitions being again determined by the degree of f-electron localization. In EuTe and YbTe the degree of f-electron localization is such that the structural transition occurs prior to the electronic transition. In SmTe and TmTe, with slightly less localized f electrons, the order of phase transitions is reversed, and the structural transition occurs after the $R^{2+} \rightarrow R^{3+}$ f-electron delocalization transition. The predicted transition pressures are overall in good agreement with experiment. The ground state predictions presented here refer

to the NaCl and CsCl structured compounds, which does not exclude the existence of an unknown yet energetically overall more stable structure.

Acknowledgments

We would like to dedicate this contribution to the memory of Professor Balazs Laszlo Gyorffy for his involvement, interest and collaboration on the electronic structure of solids with strongly localized d and f electrons using the self-interaction correction approach. He invented his own ‘brand’ of self-interaction correction, the so-called local SIC (LSIC), formulated within multiple scattering theory, where localized states are associated with sharp resonances. Utilizing an ‘alloy analogy’ and temperatures where only thermal fluctuations matter, LSIC is comparable to the LDA+ U +DMFT method. We are very grateful to Balazs for hours of enjoyable discussions and will remember him for his insight, his kindness, and his friendship.

This research used resources of the Danish Center for Scientific Computing. This work was supported by EPSRC through a service level agreement with the Scientific Computing Department of STFC.

References

- [1] Beaudry B J and Gschneidner K A Jr 1978 *Handbook on the Physics and Chemistry of Rare Earths* vol 1 ed K A Gschneidner Jr and L Eyring (Amsterdam: North-Holland)
- [2] Petit L, Tyer R, Szotek Z, Temmerman W M and Svane A 2010 *New J. Phys.* **12** 113041
- [3] Jayaraman A, Narayanamurti V, Bucher E and Maines R G 1970 *Phys. Rev. Lett.* **25** 1430
- [4] Andersen O K 1975 *Phys. Rev. B* **12** 3060

- [5] Perdew J P and Zunger A 1981 *Phys. Rev. B* **23** 5048
- [6] Temmerman W M, Svane A, Szotek Z, Winter H and Beiden S V 2000 *Lecture Notes in Physics* vol 535 ed M Dreyssé (Berlin: Springer) p 286
- [7] Svane A, Temmerman W M, Szotek Z, Lægsgaard J and Winter H 2000 *Int. J. Quantum Chem.* **77** 799
- [8] Temmerman W M, Petit L, Svane A, Szotek Z, Lüders M, Strange P, Staunton J B, Hughes I D and Gyorffy B L 2009 *Handbook on the Physics and Chemistry of Rare Earths* vol 39 ed K A Gschneidner et al (Amsterdam North-Holland) p 1
- [9] Lüders M, Ernst A, Däne M, Szotek Z, Svane A, Ködderitzsch D, Hergert W, Gyorffy B L and Temmerman W M 2005 *Phys. Rev. B* **71** 205109
- [10] Lambrecht W R L and Andersen O K 1986 *Phys. Rev. B* **34** 2439
- [11] Jomard G, Amadon B, Bottin F and Torrent M 2008 *Phys. Rev. B* **78** 075125
- [12] Larson P, Lambrecht W R L, Chantis A and van Schilfgaarde M 2007 *Phys. Rev. B* **75** 045114
- [13] Jayaraman A, Singh A K, Chatterjee A and Devi S U 1974 *Phys. Rev. B* **9** 2513
- [14] Jorgensen C K 1962 *Orbitals in Atoms and Molecules* (London: Academic)
- [15] Nugent L J 1970 *J. Inorg. Nucl. Chem.* **32** 3485
- [16] Racah G 1942 *Phys. Rev.* **62** 438
- [17] Eriksson O, Brooks M S S and Johansson B 1990 *Phys. Rev. B* **41** 7311
- [18] Methfessel M, van Schilfgaarde M and Casali R A 2000 *Lecture Notes in Physics* vol 535 ed H Dreyssé (Berlin: Springer) p 114
- [19] Svane A, Santi G, Szotek Z, Temmerman W M, Strange P, Horne M, Vaitheeswaran G, Kanchana V, Petit L and Winter H 2004 *Phys. Status Solidi b* **241** 3185
- [20] Svane A, Temmerman W M, Szotek Z, Petit L, Strange P and Winter H 2000 *Phys. Rev. B* **62** 13394
- [21] Lebègue S, Santi G, Svane A, Bengone O, Katsnelson M I, Lichtenstein A I and Eriksson O 2005 *Phys. Rev. B* **72** 245102
- [22] Svane A, Temmerman W M and Szotek Z 1999 *Phys. Rev. B* **59** 7888
- [23] Svane A, Strange P, Temmerman W M, Szotek Z, Winter H and Petit L 2001 *Phys. Status Solidi b* **223** 105
- [24] Svane A, Kanchana V, Vaitheeswaran G, Santi G, Temmerman W M, Szotek Z, Strange P and Petit L 2005 *Phys. Rev. B* **71** 045119
- [25] Svane A 2006 *Solid State Commun.* **140** 364
- [26] Temmerman W M, Szotek Z and Winter H 1993 *Phys. Rev. B* **47** 1184
- [27] Svane A, Christensen N E, Petit L, Szotek Z and Temmerman W M 2006 *Phys. Rev. B* **74** 165204
- [28] Jayaraman A 1979 *Handbook on the Physics and Chemistry of Rare Earths* vol 2 ed K A Gschneidner Jr and L Eyring (Amsterdam: North-Holland) p 575
- [29] Slater J C 1972 *Adv. Quantum Chem.* **6** 1
- [30] Harrison J G, Heaton R A and Lin C C 1983 *J. Phys. B: At. Mol. Phys.* **16** 2079
- [31] Aryasetiawan F and Gunnarsson O 1998 *Rep. Prog. Phys.* **61** 237
- [32] Anisimov V I, Zaanen J and Andersen O K 1991 *Phys. Rev. B* **44** 943
- [33] Antonov V N, Bekenov L V and Yaresko A N 2011 *Adv. Condens. Matter Phys.* **2011** 1
- [34] Antonov V N, Harmon B N, Perlov A Y and Yaresko A N 1999 *Phys. Rev. B* **59** 14561
- [35] Georges A, Kotliar G, Krauth W and Rozenberg M 1996 *Rev. Mod. Phys.* **68** 13
- [36] Wan X, Dong J and Savrasov S Y 2011 *Phys. Rev. B* **83** 205201
- [37] Rogers E, Dorenbos P and van der Kolk E 2011 *New J. Phys.* **13** 093038
- [38] Chatterjee A, Singh A K and Jayaraman A 1972 *Phys. Rev. B* **6** 2285
- [39] Tsiok O B, Sidorov V A, Bredikhin V V and Khovstantsev L G 1991 *Solid State Commun.* **79** 227
- [40] Schmiester G, Wortmann G and Kaindl G 1990 *High Pressure Res.* **3** 192
- [41] Le Bihan T, Darracq S, Heathman S, Benedict U and Mattenberger K 1995 *J. Alloys Compounds* **226** 143
- [42] Jarrige I et al 2013 *Phys. Rev. B* **87** 115107
- [43] Gupta D C and Kulshrestha S 2009 *J. Phys.: Condens. Matter* **21** 436011
- [44] Rooymans C J M 1965 *Solid State Commun.* **3** 421
- [45] Singh S, Jayaraman A and Chatterjee A 1971 *Solid State Commun.* **9** 1459
- [46] Goncharenko I N and Mirebeau I 1997 *Europhys. Lett.* **37** 633
- [47] Kong B, Zhou Z W, Sun X W, Zhang L and Ling-Hui R F 2013 *Acta. Phys. Pol. A* **123** 720
- [48] Léger J M, Epain R, Loriers J, Ravot D and Rossat-Mignod J 1983 *Phys. Rev. B* **28** 7125
- [49] Zvoriste-Walters C E, Heathman S and Klimczuk T 2013 *J. Phys.: Condens. Matter* **25** 265401
- [50] Heathman S, Le Bihan T, Darracq S, Abraham C, De Ridder D J A, Benedict U, Mattenberger K and Vogt O 1995 *J. Alloys Compounds* **230** 89
- [51] Tang J, Kosaka T, Matsumura T, Matsumoto T, Mōri N and Suzuki T 1996 *Solid State Commun.* **100** 571
- [52] Matsumura T, Kosaka T, Tang J, Matsumoto T, Takahashi H, Mōri N and Suzuki T 1997 *Phys. Rev. Lett.* **78** 1138
- [53] Chatterjee A, Singh A K, Jayaraman A and Bucher E 1971 *Phys. Rev. Lett.* **27** 1571
- [54] Jarrige I, Rueff J P, Shieh S R, Taguchi M, Ohishi Y, Matsumura T, Wang C P, Ishii H, Hiraoka N and Cai Y Q 2008 *Phys. Rev. Lett.* **101** 127401
- [55] Devi S U and Singh A K 1984 *Solid State Commun.* **52** 303
- [56] Suryanarayanan R, Ferré J and Briat B 1974 *Phys. Rev. B* **9** 554
- [57] Hurych Z, Wang C C and Wood C 1971 *Phys. Lett. A* **34** 291
- [58] Francillon M, Jérôme D, Achard J C and Malfait G 1970 *J. Physique* **31** 709
- [59] Léger J M, Oki K, Ravot D, Rossat-Mignod J and Vogt O 1985 *J. Magn. Magn. Mater.* **47–48** 277
- [60] Temmerman W M, Svane A, Petit L, Lüders M, Strange P and Szotek Z 2007 *Phase Transitions* **80** 415
- [61] Vaitheeswaran G, Petit L, Svane A, Kanchana V and Rajagopalan M 2004 *J. Phys.: Condens. Matter* **16** 4429
- [62] Syassen K 1986 *Physica B* **139–140** 277
- [63] Jia Y Q 1991 *J. Solid State Chem.* **95** 184
- [64] Strange P, Svane A, Temmerman W M, Szotek Z and Winter H 1999 *Nature* **399** 756